SYNTHESIS AND STRUCTURAL CHARACTERIZATION OF BISMUTH-TIN NANOPARTICLES IN A POLYMER MATRIX

OSCAR JAVIER SUAREZ [1], JHON JAIRO OLAYA [1], JOSE EDGAR ALFONSO [2]

[1] Grupo de Análisis de fallas e Integridad y Superficies, Facultad de Ingeniería Universidad Nacional de Colombia, Cra 45 No 26-85, Bogotá DC, Colombia.

[2] Grupo de Ciencia de Materiales y Superficies, Dpto. de Física Universidad Nacional de Colombia, Cra 45 No 26-85, Bogotá DC, Colombia.

e-mails: ojsuarezg@unal.edu.co. jealfonsoo@unal.edu.co, jjolayaf@unal.edu.co.

Recibido: julio 2015 Aprobado para publicación: marzo 2016

ABSTRACT

Nanostructured materials Bi and Si have a potential application as electrodes for detecting heavy metals via electro-analytical techniques such as the separation voltammetry. In this work nanocomposites stable polymer / metal bismuth and tin type were obtained using ultrasonic radiation in dimethylformamide and as a stabilizer a nonionic surfactant. The hydrodynamic diameter of the particles in solution was measured by the technique of dynamic light scattering (DLS), the results showed about 100 nm diameter with low polydispersity for nanocomposites of tin and a bigger size for the bismuth. Nanocomposite films were obtained at 353 and 393 K, the analysis of morphology, composition and microstructure were made by scanning electron microscopy (SEM) coupled with probe EDX and X-ray diffraction (XRD) respectively. The XRD diffraction patterns show different trends of crystallization for the two metals in nanocomposites: amorphous bismuth, and crystalline tin.

Keywords: bismuth, tin, nanoparticles, polymer nanocomposites, crystallinity

SÍNTESIS Y CARACTERIZACIÓN ESTRUCTURAL DE NANOPARTICULAS DE BISMUTO-ESTAÑO EN UNA MATRIZ POLIMÉRICA

RESUMEN

Los materiales nanoestructurados de Bi y Sn tienen una potencial aplicación como electrodos en la detección de metales pesados a través de técnicas electro-analíticas tales como la voltametría de separación. En este trabajo se obtuvieron nanocompuestos estables del tipo polímero/metal de bismuto y estaño usando radiación ultrasónica en dimetilformamida y utilizando como estabilizante un tensoactivo no iónico. El diámetro hidrodinámico de las partículas en solución se midió mediante la técnica de dispersión de luz dinámica (DLS), los resultados mostraron un diámetro cercano a los 100 nm con baja polidispersidad para los nanocompositos de estaño y un tamaño mayor para el bismuto. Se obtuvieron películas de los nanocompuestos a 353 y 393 K, los análisis de morfología, composición y microestructura se hicieron por medio de microscopía electrónica de barrido (SEM) con sonda EDX acoplada y difracción de rayos X (XRD) respectivamente. Los patrones de difracción de XRD muestran diferentes tendencias de cristalización para los dos metales en los nanocompuestos: el bismuto amorfo y el estaño cristalino.

Palabras clave: bismuto, estaño, nanopartículas, nanocompositos poliméricos, cristalinidad

INTRODUCTION

Metal/Polymer composite materials exhibit intermediate properties among their components. The polymeric matrix provides qualities such as processability, dispersability or thermal stability, while metal provides electronic, magnetic, or catalytic properties (Balan and Burget 2006; Nicolais and Carotenuto, 2005). Metalic nanoparticles (MNPs) may be considered as being in an intermediate situation between bulk metals and the atoms that compose them. Due to their small size, they exhibit different properties (electric, magnetic, optical and catalytic) from the macroscopic metal and the isolated atoms. However these properties may be transient. This means that inestability is possible for this

kind of particle, so the stabilization of MNPs is needed for the following reasons: to avoid an uncontroled growth of the particles, to avoid coagulation, to control the growth rate and the final size, as well as to allow stable dispersions of the partciles in different solvents (Benito 2006; Muraviev *et al.* 2006; Nicolais and Carotenuto 2005).

Different means have been employed for the synthesis of nanoparticles in a polymer matrix, almost all based on reactions in situ, where the particles are generated from the metallic precursor in the precence of the polymeric material, which sometimes acts as a nanoreactor (Balan and Burget 2006; Benito 2006; Kargin et al, 2006; Muraviev et al, 2006). The various procedures employed for the metal reduction are: chemical, thermal, photochemical, and electrochemical reduction. The material can be pulverized or melted on a substrate for subsequent applications.

The stabilization mechanisms of nanoparticles can be classified into electrostatic, steric, and a combination of the two. The first is based on the separation of electric charges due to the formation of an electrical double layer around the particles, while the second is based on geometric and spatial repulsion due to the large size of the adsorbed molecules on the nanoparticle surface (Kraynov and Müller n.d.).

The production of charges on the metallic surface may occur due to the presence of ionogenic groups or the adsorption of ionic surfactants. Unfortunately, this mechanism is not sufficient in practice because of the high concentration of electrolyte usually employed. An alternative is the use of nonionic surfactants or polymeric surfactants such as polyvinyl pyrrolidone, polyaniline or polyethylene oxides (Anno et al, 2009; Wang et al, 2008) as well as ionic liquids, although the latter exhibit strong coordination which is good for applications in physics, such as quantum dots but not for catalysis or sensors, where access to the metallic surface is required (Kraynov and Müller n.d.).

Crystallization of the nanoparticles involves a surface and a thermodynamic process. The energy change for particle growth (ΔG_{TOT}) is given by Equations 1 and 2:

$$\Delta G_{TOT} = \Delta G_S + \Delta G_b \quad (1)$$

$$\Delta G_{TOT} = 4\pi r^2\sigma + \tfrac{4}{3}\pi r^3\left(kTln\Delta\mu\right) \quad (2)$$

where σ is the surface energy, k the Boltzmann constant, T the absolute temperature, r the particle radius, and $\Delta\mu$ is called the supersaturation defined as the ratio between the actual concentration of the species and its equilibrium concentration (Yoreo and Vekilov 2003).

ΔG_s increases due to increases of surface particles (second power of the radius) while ΔG_b decreases due to the formation of a bulk material (third power of radius). The minimal radius of the crystallite is known as the critical size **r***, and only nuclei that reach this value survive. In the production of nanoparticles this value represents how small nanoparticles can be synthetized and can be calculated when $\Delta G_{TOT}/dr = 0$.

$$r^* = 2\sigma/\Delta G_b \quad (3)$$

The energy of the crystal at the critical size (ΔG*) is equivalent to an energy barrier that must be overcome in order to obtain continuous growth, and can be obtained by derivation of the total expression. The obtained result shows that the energy of the crystal depends on the surface energy and the super saturation (Yoreo and Vekilov 2003).

$$\Delta G^* \propto \sigma^3/\Delta\mu^2 \quad (4)$$

This energy barrier is higher for more stable states, which means that it is likely that initially unstable species are formed. These structures initially formed will vary over time in order to achieve the most stable state.

Some works have been reported for producing metallic nanoparticles by techniques such as chemical, electrochemical or thermal reduction using different methods for stabilizing the nanoparticles (Anandan, Asiri, and Ashokkumar 2014; Anno et al, 2009; Chee and Lee 2012; Jiang et al, 2006; Kargin *et al.* 2006; Wang et al, 2008).

The main objective of this investigation is to be an initial step in the development of nanostructured bismuth and tin materials to be used as electrodes, as proposed by Wang and other researchers (Pan *et al.* 2011; Wang and Lu 2001; Wang *et al.* 2000).

MATERIALS AND METHODS

Metal nanocomposite synthesis

Metallic nanoparticles were produced by chemical reduction of salts precursor (bismuth and tin chlorides Aldrich/Merck) with sodium borohydride (Merck). Sulfonated styrene-divinylbenzene copolymer called P4 and P5 (previously synthetized and selected in our laboratory) and Nafion were used as steric stabilizers while polyethylene glycol dodecyl ether 70% (Brij 35-Fisher) was used as electrostatic stabilizer, all reagents were dissolved in dimethylformamide

(Aldrich). Cup horn sonicator BRANSON 250 was employed for ultrasonic radiation: 20% amplitude (44W) and 10 min of sonication time were predetermined. When sonication started, 0.5 mL of reducing solution was quickly added to 3 mL of reactive mix. The composition in the final reactive mix was: nonionic surfactant 7 mM, total metal content 2 mM and reducing agent 10 mM. Half reactions involved are given by equations 5-7.

Reduction:

$$Sn^{+2} + 2e^- \longrightarrow Sn^0 \quad (E^o = -0.14V) \tag{5}$$

$$Bi^{+3} + 3e^- \longrightarrow Bi^0 \quad (E^o = 0.308) \tag{6}$$

Oxidation:

$$BH_4^- + 8OH^- \longrightarrow B(OH)_4^- + 4H_2O + 8e^- \quad (E^o = -0.48V) \tag{7}$$

Characterization

Films of metal/polymer nanocomposites were prepared by casting on glass substrates and dried at 353K and 393K for structural characterization and on graphite (dried at 393K) for electrochemical measurements.

Dynamic light scattering (DLS) was used for measuring the hydrodynamic particle distribution diameter of the metal-polymer nanocomposite in a solution using a Zetasizer NanoZS. For this purpose 0.3 mL of nanocomposite solution was dissolved up to 1.0 mL with DMF and stabilized for 120 s at 298 K in a glass cell.

X-ray diffraction (XRD) was used for determination of the microstructure on an X-PertPro Panalitycal, Bragg-Brentano configuration Θ-2Θ from 10° to 70°, with a step of 0.02°, and copper Kα radiation (0.154 nm). The size of the crystallite in nanocomposite films can be calculated using the Debye-Scherer equation (Eq. 8)

$$\beta = \frac{K\lambda}{D\cos\theta} + \frac{4\varepsilon sen\theta}{\cos\theta} \tag{8}$$

where β is the mean crystallite size, λ the incident radiation of CuKα, θ the Bragg angle, K a constant (0.9), and ε the micro deformations. The second term on the right side of the equation corresponds to the contribution due to residual stresses. This can be assumed to be zero for this case, due to the fact that the metal particles are isolated from each other in a polymer matrix and can be taken to be a metal powder.

Cyclic voltammetry was made in an AUTOLAB system using an Ag/AgCl reference electrode in a solution of acetate buffer (pH 5.0) with and without addition of 60 µg/L of cadmium.

RESULTS AND DISCUSSION

Solutions of all reactants in DMF were translucent, except BiCl3 which exhibited poor solubility in DMF and must be sonicated for good dispersion before reaction. After the addition of the reducing agent, all the solutions change their transparent color to: black for bismuth, dark brown for tin-bismuth, and amber for tin.

Nanocomposites obtained with copolymer P4 were always darker than with the P5 copolymer solutions, and Nafion solutions were the brightest of all. Bismuth/Nafion MNPs was the most stable of the bismuth solutions prepared. In P4 and P5 copolymers, Bi was unstable and precipitated as a dark powder after a few days, while all tin and bismuth-tin MNPs solutions maintained their color and appearance for many weeks and months.

Suspensions of metal polymer nanocomposites in DMF were analyzed via DLS in order to determine the hydrodynamic size distribution of the particles formed. Solutions of DMF with only surfactant (Brij) and with the mixed surfactant-copolymer were also evaluated for comparison, and are shown in figure 1a. The results show varied behavior for the copolymer solutions. An unimodal distribution for brij and nafion (mean diameter 133 nm and 216 nm respectively), a bimodal distribution for P4 solutions with mean diameters of 562 and 84 nm, and a trimodal distribution for P5 with peaks at 413, 68, and 15 nm can be seen. This multimodal size distribution of synthesized copolymers possibly indicates high dispersity in the size and molecular weight of these materials.

In figure 1b, details of the size distributions of MNPs suspensions obtained with the copolymer P5 can be observed. The bismuth particles in P5 are larger than others, including those of the same metal in Nafion and in copolymer P4 (figure 2) and also exhibit a bimodal distribution. This larger size of bismuth particles can cause the prompt precipitation of metal observed in this case. Tin and tin-bismuth solutions in P5 copolymer exhibit mean diameters of particles, close to 100 nm. The smaller particle size in the latter cases is responsible for the lasting stability of tin MNPs solutions.

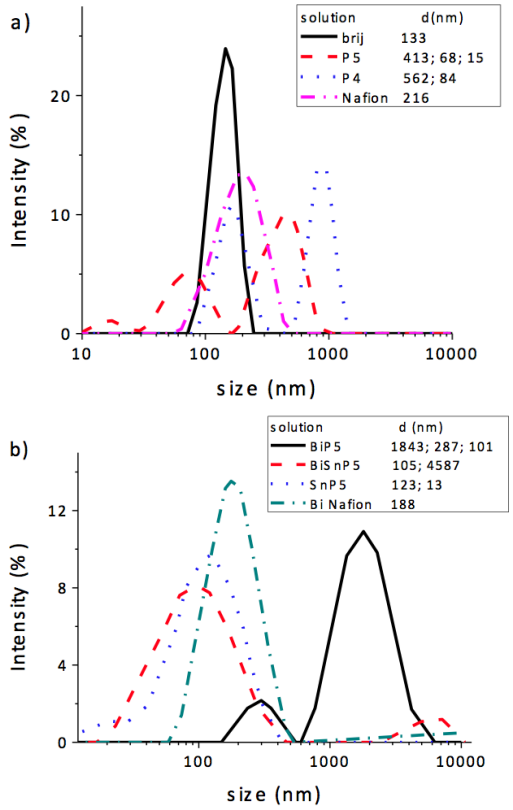

Figure 1. *Size distribution of: a) copolymers and b) Bi-copolymer nanocomposite solutions*

Figure 2 shows the mean diameter of particles obtained by other systems of metal/polymer suspensions. It can be seen that except for bismuth solution copolymers, all the solutions exhibit a principal peak with medium diameter close to 100 nm, which confirms the existence of metal-polymer nanoparticles suspended in DMF.

The mean diameter and the width of the principal peak are shown in table 1. There it is shown that the presence of tin seems to have an effect on the size of metal nanoparticles, leading to a smaller and narrower distribution.

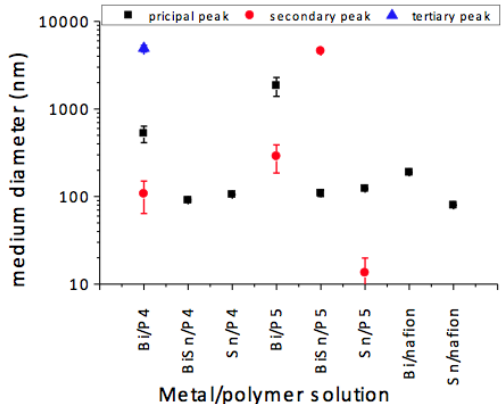

Figure 2. *Medium diameter of particles for metal-polymer nano-composite solutions (DLS)*

The growth of nanocrystals from a solution involves two important processes: the nucleation, followed by growth of the nanocrystals. Lifshitz (Lifshitz and Slyozov, 1961) and Wagner *et al.*, in 1961 and later Rao *et al.*, in 2007 proposed a model for the growth of nanoparticles (The LSW model) that can predict the radius of nanoparticles as a function of time based on a supposition of a stationary state of the system and derived from Fick´s law. The final equation (eq. 9) predicts that the radius depends on the cube root of the time and a constant, *K*.

$$r^3 - r_0^3 = Kt \qquad (9)$$

where K depends on the molar volume (V_m), diffusion coefficent (D), surface energy of the metal (σ), concentration of the metal (C_∞), and temperature (T).

$$K = \frac{g v_m^2 D \sigma C_\alpha}{9RT} \qquad (10)$$

Replacing average values for B_i and Sn in equations 9 and 10, with mean values of σ: Bi = 0.54 J/m and Sn = 0.62 J/m (Vitos *et al.* 1998) and the molar volume with 0.02137 m^3/kmol and 0.01631 m^3/kmol for bismuth and tin respectively, it can be observed that the model predicts that smaller stable particles can be obtained from tin than with bismuth. A synergy between smaller value of the molar volume of tin and higher density of Bi (9780 kg/m^3), and also the greater size of the particles of synthesized copolymers, whose function is to stabilize the metal MNPs, can play a role in the rapid growth and precipitation of Bi particles.

XRD was performed on the films of nanocomposites after they were dried at 353 and 393 K on a glass substrate, in order to observe the composition of metal MNPs and changes in microstructure after casting films at different temperatures. No peaks clearly defined for the nanoparticles of Bi (figure 3) in copolymers P4 and P5 obtained at 353 and 393 K were observed in the diffraction pattern for Bi nanocomposite films, this could be caused by formation of an amorphous material. However in the nanocomposite synthetized with Nafion, characteristic planes (012) and (110) were observed at 27.3° and 39.8°, which is similar to reported results (Anno *et al.* 2009; Kong *et al.* 2014; Lien *et al.* 2013; Mayorga-Martinez *et al.* 2013; Yang *et al.* 2013). Also, in these papers it was recognized that the parameters used during production can affect the preferential planes formed. When Bi/Nafion film was dried at 393K, the (012) peak became sharper and plane (104) appeared, which probably means that a recrystallization process can occur at this temperature. Other peaks corresponding to some components of the solution can be seen, for example: (200)

at 31.7°, corresponding to NaCl, and (001), (102) and (003) at 12, 24.2, and 36.6° respectively, corresponding to BiOCl. The appearance of these ones means that incomplete reduction of bismuth occurs during the reaction.

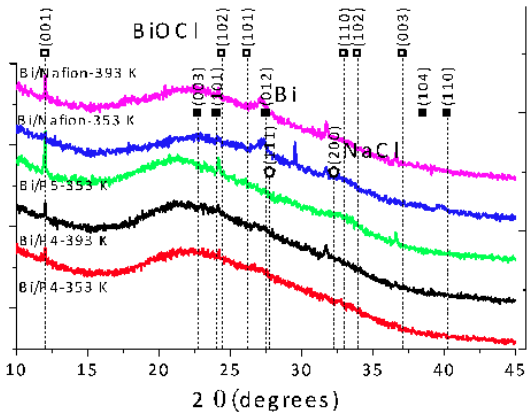

Figure 3. *XRD patterns for films of Bi/polymer nanocomposites and comparison with reference patterns (Bi PDF 00-005-0519)*

Figure 4 shows XRD patterns for tin nanocomposites. Peaks of surfactant (Brij) appear at 19 and 23°, while the peaks corresponding to the βSn phase also appear, indicating a crystalline structure of this metal. For the nanocomposite Sn/P4 dried at 353K, planes corresponding to (101), (200), and (211) can be observed. After casting at 393K, new planes (202) and (220) appear. These new planes also confirm a possible recrystallization process for tin at 393K, as with Bi/Nafion. For the nanocomposite Sn/P5, the (110) at 21,4° is also observed, while for nanocomposites of tin with nafion, only planes (101) and (202) can be seen.

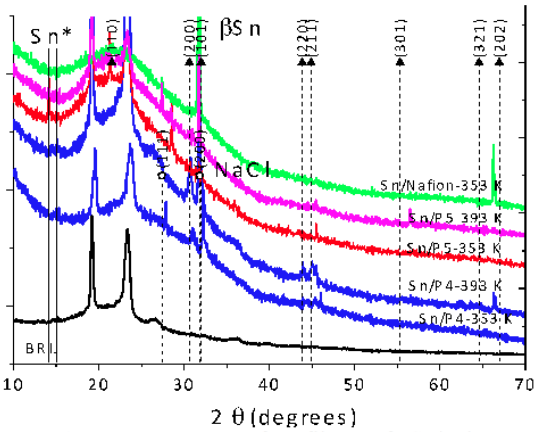

Figure 4. *XRD patterns for films of Sn/polymer nanocomposites and comparison with reference patterns (Sn PDF 03-065-0296)*

Figure 5 shows the XRD patterns for Bi-Sn film nanocomposites. For the nanocomposite BiSn/P4, the characteristic plane (012) at 27.3° for bismuth can be seen in both films obtained at 353 and 393K, which indicates that the tin could influence the crystallization process for bismuth. The planes (101) and (202) corresponding to βSn also appear for all the nanocomposites. However, the peak for the (202) plane became sharper when the films were dried at 393 K. The nanocomposite BiSn/P5 also shows growth of the (110) plane for tin, as occurred with the Sn/P5 film. This also indicates that the polymeric matrix interacts with the metal and affects the crystallization process, changing the preferential growth planes. Specific crystallographic orientation is difficult to explain without resorting to active controls during the nucleation stage. Some examples in nature have been reported that suggest that the crystallization is controlled by the presence of organic components, such as proteins and other organic molecules, which serve as templates, providing preferential sites for nucleation and controlling the orientation of the resulting crystals, as occurred with β-sheet polyaspartate adsorbed onto sulfonated polystyrene substrates, which induced nucleation of (001) oriented calcite crystals (Yoreo and Vekilov 2003).

Crystallite size calculated from the principal diffraction peak for each nanocomposite is shown in table 3. Changes observed in the preferential planes and a small change in the crystallite size can indicate a recrystallization process of metals in the films obtained at 393K as compared to those obtained at 353K. As can be seen in the same table, the crystallite size of tin and the medium hydrodynamic size of the particles in the solutions are something different; however, the values are on the same order of magnitude close to 100 nm.

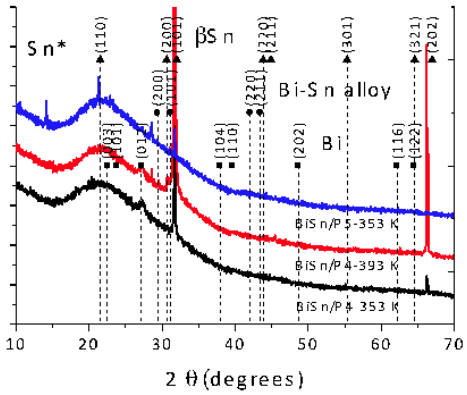

Figure 5. *XRD patterns for films of BiSn/polymer nanocomposites and comparison with reference patterns (Bi-Sn alloy PDF 03-065-5432)*

As can be seen in equations 3 and 4, the critical size and the energy barrier of crystal is proportional to the surface energy and inversely proportional to the supersaturation. To obtain a small crystallite size, as occurred with bismuth, there are two possibilities: a smaller value of the surface energy or a higher value of the supersaturation.

Comparison between the mean surface energies reported for tin and bismuth (Vitos et al, 1998) shows that it is 14% higher for tin. This difference implies a smaller critical radius for bismuth, but not enough to form an amorphous material. On the other hand, the growth of metals obtained by chemical reduction can be described as following (Lin et al, 2013):

Step 1:

$$M^{a+}_{solution} + ae^{-} \xrightarrow{\theta} M_{solution(\mu s)} \qquad (11)$$

Step 2:

$$M_{solution(\mu s)} \xrightarrow{\Delta\mu} M_{crystal(\mu c)} \qquad (12)$$

The metal precursor (M^{a+}) should first be reduced to metallic atoms by step 1 (Eq. 11), whose speed is given by υ, and then the metallic atoms grow on the crystallites during step 2 (eq. 12), which is driven by the supersaturation ($\Delta\mu$).

From the above equations, it can be seen that the chemical potential of reduced metallic atoms in a solution (μ_s) will increase with an increase in the metal reduction rate (υ). So it can be expected that the supersaturation ($\Delta\mu$) of metal atoms, defined as the difference of chemical potentials of metal atoms between the solution phase (μ_s) and the solid phase (μ_c), will increase with an increase in the metal reduction rate.

The reduction rate is given by the electrochemical kinetics, so the rate depends exponentially on the polarization, which is defined as the difference between the reaction potential and the potential of the equilibrium reaction. It is known that polarization increases when the equilibrium potential difference for half reactions increases. In this case, it is expected that greater differences between equilibrium potential reactions exist for bismuth/hydride (ΔE^o=0.788V) than for tin/hydride (ΔE^o=0.340 V). The exponential dependence on polarization can cause large differences of supersaturation between tin and bismuth. Higher values of $\Delta\mu$ for bismuth during reduction could be a reasonable cause to better explain the amorphous phase vs. crystalline material for tin.

The morphology of the nanocomposite films is shown in figure 6. Figures 6a and 6b are secondary electron images at 1.5 kX, and show the morpology of Sn/P4 films obtained at 353 and 393 K. An irregular surface can be seen, similar to the one previously observed in figures for copolymers only. For the films obtained at 393 K, the formation of pores can also be observed, which could be caused by an increased evaporation rate of the solvent at this temperature. In figure 6c, a backscatering electron image for the Sn/Nafion film produced at 353K is shown. In this image, a smooth surface and no contrast in the composition can be observed. However, EDX analysis (not shown) shows the presence of tin, silicon, carbon, oxygen, chlorine, and sodium. All these elements are components of the substrate, the polymer, and the precursor used during synthesis.

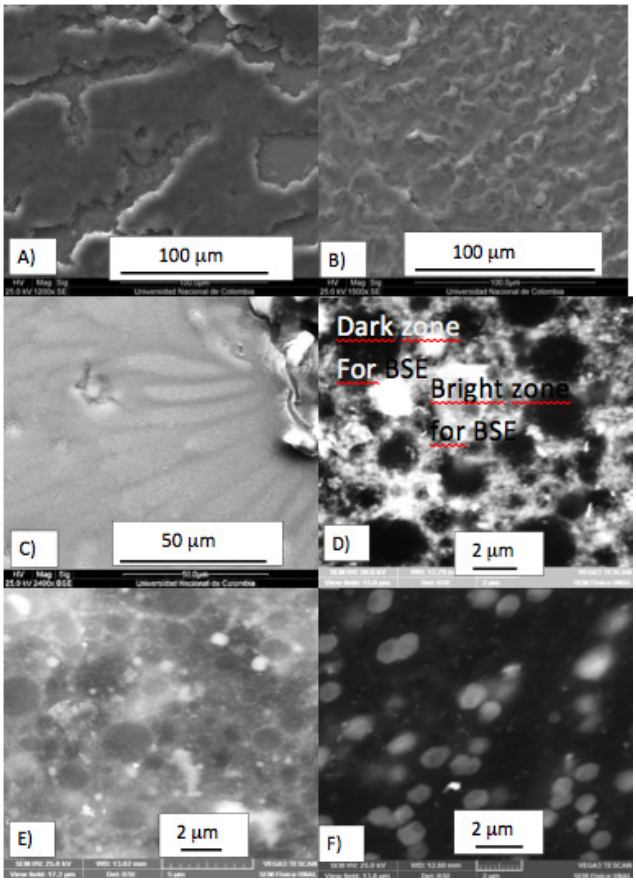

Figure 6. *SEM micrographs for films of metal-copolymer nanocomposites; A)Sn/P4-353 K; B)Sn/P4-393 K; C)Sn/Nafion-353 K; D)Bi/P5-353 K; E)Sn/P5-353 K; F) Bi/Nafion-393 K*

Figures 6d to 6f were captured with backscatering electrons at high magnification (10 kX), and correspond to Bi/P5-353K, Sn/P5-353K, and Bi/Nafion-393K respectively. A contrast between dark zones (polymer rich) and bright zones

(metal rich) can be seen. The EDX analysis for Bi/P5-353 K in both zones, dark and bright, are shown in figure 7. For all nanocomposites, lower or no detection of metal in the dark zones was observed, while metal is present at between 5 and 15 % of weight in the bright zones.

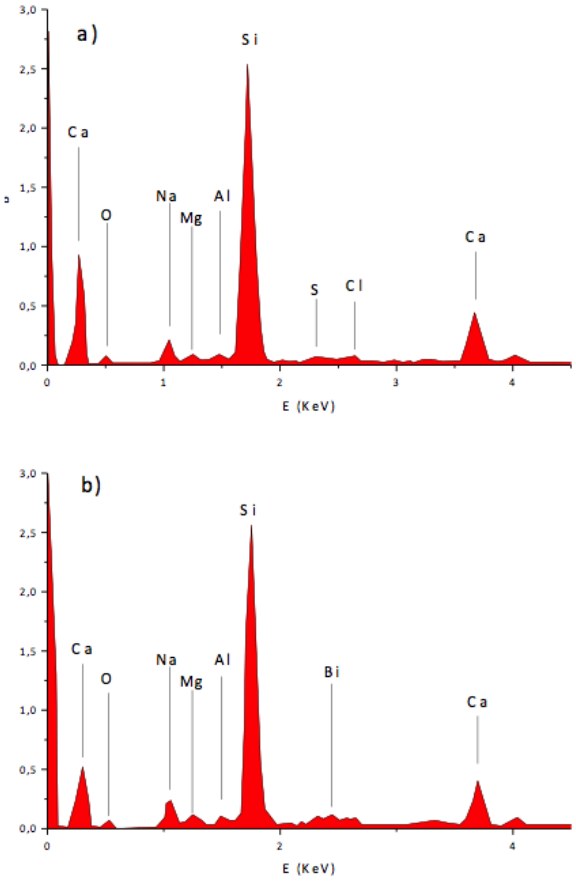

Figure 7. *EDX spectra for Bi/P5-353 K in a) dark zone and b) bright zone*

Bright zones observed in figure. 6d for Bi/P5-353 K nanocomposite correspond to clusters of metal nanoparticles, while individual particles of between 200 and 500nm can be observed for Sn/P5 at 353K and Bi/ Nafion at 393K. This confirms the larger size of particles obtained for Bi/P5, which causes quick precipitation.

The electrochemical response of Bi and Sn nanocomposites deposited on a graphite surface and evaluated in a solution of acetate buffer pH 5.0 are presented in figure 8. For cyclic voltammetry of nanocomposites in buffer solutions without Cd, not waves due to faradaic process were observed as expected. However, when cadmium is added to the solution, a peak with wave form can be observed for the Bi/P4 nanocomposite, this behaviour is not observed for other metal-polymer nanocomposites or graphite, which means that Bi nanoparticles in P4 copolymer have good electrochemical response with potential for being employed in heavy metals detection.

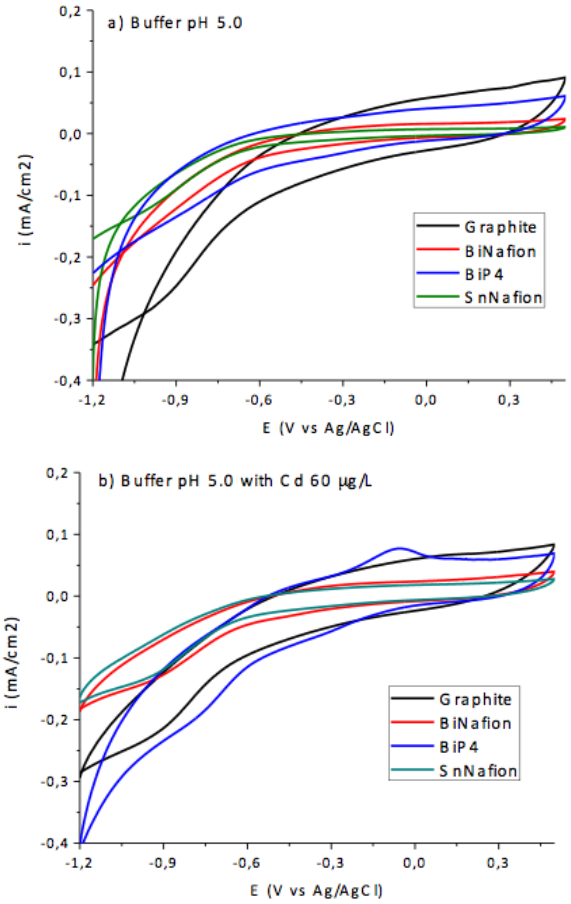

Figure 8. *Cyclic voltammetry curves for selected metal/ polymer nanocomposites at scan rate 100 mV/s. in: a)acetate buffer pH 5.0; b) acetate buffer pH 5.0 plus Cd 60 µg/L*

Table 1. Hydrodynamic particle size (DLS) and metal crystallite size (XRD)

Nanocomposite	Hydrodynamic particle diameter (DLS)		Crystallite size (XRD)		
	Medium diameter of principal peak (nm)	Medium width of peak (nm)	Plane (hkl)	Film at 353 K	Film at 393 K
Bi/P4	524	251	None	---	---
BiSn/P4	91	43	Bi (012) Sn (101)	13 141	13 170
Sn/P4	105	63	Sn (101)	170	101
Bi/P5	1843	682	None	---	Non measured
BiSn/P5	109	81	Sn (101) BiSn (200)	134 91	Non measured
Sn/P5	123	71	Sn (…)	110 (110)	103 (101)
Bi/Nafion	189	80	Bi (012)	12	13
Sn/Nafion	80	31	Sn (101)	159	Non meassured

CONCLUSIONS

Metal/copolymer nanocomposites with Bi, Sn and Bi-Sn mixtures were synthesized by chemical reduction in a nonionic surfactant – polymer solution (P4, P5, and Nafion) using DMF as a solvent and ultrasonic irradiation to help maintain a small distribution of particle size. Sn and Bi-Sn solutions were stable while Bi metal solutions were less stable over time.

The hydrodynamic particle diameter measured via dynamic light scattering showed that suspensions of metal/polymer nanocomposites exhibited different distributions with respect to their polymer precursors; however the final particle size was influenced by the polymer particle size. The largest size and a lower stability for Bi particles can be explained by the synergy between the greater polymer size and the physical properties of bismuth, which results in rapid particle growth and coagulation.

X-ray diffraction of films of metal/polymer nanocomposites obtained after drying at 353K and 393K showed that there must be a polymer –metal interaction that modifies the growing planes during the recrystallization process at different temperatures. An amorphous structure for Bi was observed, which could be caused by differences in the kinetic reduction rates. Also a possible recrystallization process was observed when comparing the results obtained at 353 K with those at 393 K.

At higher magnification it was possible to observe different phases in the nanocomposites as a contrast in the composition between polymer rich zones and metal rich zones. These nanostructured Bi-Sn materials could be studied for possible use as coating electrodes for application in electro analytical techniques.

ACKNOWLEDGEMENTS

Bisnano Project, COLCIENCIAS, and Universidad Nacional de Colombia for financial support.

REFERENCES

Anandan, S., Asiri, A. M. and Ashokkumar,. M (2014). "Ultrasound assisted synthesis of Sn nanoparticles-stabilized reduced graphene oxide nanodiscs." Ultrasonics sonochemistry 21(3):920–23. Retrieved May 13, 2014 (http://www.ncbi.nlm.nih.gov/pubmed/24262757).

Anno, H.Fukamoto, M., Heta, Y., Koga, K., Itahara, H. 2009. "Preparation of Conducting Polyaniline-Bismuth Nanoparticle Composites by Planetary Ball Milling." Journal of Electronic Materials 38(7):1443–49.

Balan, L. and D. Burget. 2006. "Synthesis of Metal/polymer Nanocomposite by UV-Radiation Curing." European Polymer Journal 42(12):3180–89. Retrieved November 5, 2012 (http://linkinghub.elsevier.com/retrieve/pii/S0014305706002849).

Benito, Jorge Macanas de. 2006. "Desarrollo de Nuevas Membranas Para La Separación de Iones Metálicos Y Aplicaciones Electroquimicas." Universidad Autonoma de Barcelona.

Chee, Sang-Soo and Jong-Hyun Lee. 2012. "Reduction Synthesis of Tin Nanoparticles Using Various Precursors

and Melting Behavior." Electronic Materials Letters 8(6):587–93. Retrieved May 6, 2014 (http://link.springer.com/10.1007/s13391-012-2086-y).

Jiang, Hongjin, Kyoung-sik Moon, Hai Dong, Fay Hua, and C. P. Wong. 2006. "Size-Dependent Melting Properties of Tin Nanoparticles." Chemical Physics Letters 429(4-6):492–96. Retrieved May 13, 2014 (http://linkinghub.elsevier.com/retrieve/pii/S0009261406011699).

Kargin, Yu. F. *et al.* 2006. "Preparation of Bismuth Nanoparticles in Opal Matrices through Reduction of Bismuth Compounds with Supercritical Isopropanol." Inorganic Materials 42(5):487–90.

Kong, Dandan *et al.* 2014. "Pre-Plating of Bismuth Film Electrode with Coexisted Sn2+ in Electrolyte." Electrochimica Acta 125:573–79. Retrieved (http://dx.doi.org/10.1016/j.electacta.2014.01.100).

Kraynov, Alexander and Thomas E. Müller. n.d. "Concepts for the Stabilization of Metal Nanoparticles in Ionic Liquids."

Lien, C., Hu, C., Chang, K., Tsai, Y., & Wang, D. S. (2013). A study on the key factors affecting the sensibility of bismuth deposits toward Sn2 : Effects of bismuth microstructures on the Sn2 pre-deposition. Electrochimica Acta, 105, 665-670. Retrieved (http://dx.doi.org/10.1016/j.electacta. 2013.04.121).

Lifshitz, L. and Slyozov, V. (1961). "The Kinetics of Precipitation from Supersaturated Solid Solutions." Journal of Physics and Chemistry of Solids 19(1):35–50.

Lin, H., Lei, Z., Jiang, Z., Hou, C., Liu, D., Xu, M., Xie, Z. (2013). Supersaturation-Dependent Surface Structure Evolution: From Ionic, Molecular to Metallic Micro/Nanocrystals. J. Am. Chem. Soc. Journal of the American Chemical Society, 135(25), 9311-9314.

Mayorga-Martinez, C. C., Cadevall, M., Guix, M., Ros, J., & Merkoçi, A. (2013). Bismuth nanoparticles for phenolic compounds biosensing application. Biosensors and Bioelectronics, 40(1), 57-62. Retrieved May 27, 2014 (http://www.ncbi.nlm.nih.gov/pubmed/22809524).

Muraviev, Dmitri N., Jorge Macanás, Marinella Farre, Maria Muñoz, and Salvador Alegret. 2006. "Novel Routes for Inter-Matrix Synthesis and Characterization of Polymer Stabilized Metal Nanoparticles for Molecular Recognition Devices." Sensors and Actuators B: Chemical 118(1-2):408–17. Retrieved October 29, 2012 (http://linkinghub.elsevier.com/retrieve/pii/S092540050600325X).

Nicolais, Luigi and Gianfranco Carotenuto. 2005. Metal-Polymer Nanocomposites. edited by Luigi Nicolais and Gianfranco Carotenuto. Hoboken, NJ, USA: John Wiley & Sons, Inc. Retrieved (http://doi.wiley.com/10.1002/0471695432).

Pan, Dawei, Li Zhang, Jianmei Zhuang, Tanji Yin, and Wei Qin. 2011. "A Novel Tin-Bismuth Alloy Electrode for Anodic Stripping Voltammetric Determination of Zinc." Microchimica Acta 177(1-2):59–66. Retrieved October 23, 2012 (http://www.springerlink.com/index/10.1007/s00604-011-0749-2).

Vitos, L., A. V Ruban, H. L. Skriver, and J. Kolla. 1998. "The Surface Energy of Metals." Srface Science 411:186–202.

Wang, Fudong *et al.* 2008. "Size- and Shape-Controlled Synthesis of Bismuth Nanoparticles." chem mater 20:3656–62.

Wang, J., J. Lu, Sb Hocevar, Pa Farias, and B. Ogorevc. 2000. "Bismuth-Coated Carbon Electrodes for Anodic Stripping Voltammetry." Analytical chemistry 72(14):3218–22. Retrieved (http://www.ncbi.nlm.nih.gov/pubmed/10939390).

Wang, Joseph and Jianmin Lu. 2001. "Stripping Voltammetry with the Electrode Material Acting as a ` Built-in ' Internal Standard U Anik Kirg." Electrochemistry Communications 3:703–6.

Yang, Haifeng, Junfang Li, Xiaojing Lu, Guangcheng Xi, and Yan Yan. 2013. "Reliable Synthesis of Bismuth Nanoparticles for Heavy Metal Detection." Materials Research Bulletin 48(11):4718–22. Retrieved April 30, 2014 (http://linkinghub.elsevier.com/retrieve/pii/S0025540813006740).

Yoreo, James J. De and Peter G. Vekilov. 2003. "Principles of Crystal Nucleation and Growth." Reviews in mineralogy and geochemistry 54:57–90.